Variance Reduction in a Dataset of Normal Macular Ganglion Cell Plus Inner Plexiform Layer Thickness Maps with Application to Glaucoma Diagnosis

Robert W. Knighton,[1] *Giovanni Gregori,*[1] *and Donald L. Budenz*[2]

Purpose. To examine the similarities and differences in the shape of the macular ganglion cell plus inner plexiform layers (GCL+IPL) in a healthy human population, and seek methods to reduce population variance and improve discriminating power.

Methods. Macular images of the right eyes of 23 healthy subjects were obtained with spectral domain optical coherence tomography. The thickness of GCL+IPL was determined by manual segmentation, areas with blood vessels were removed, and the resulting maps were fit by smooth surfaces in polar coordinates centered on the fovea.

Results. The mean GCL+IPL thickness formed a horizontal elliptical annulus. The variance increased toward the center and was highest near the foveal edge. Individual maps differed in foveal size and overall GCL+IPL thickness. Foveal size correction by radially shifting individual maps to the same foveal size as the mean map reduced perifoveal variance. Thickness alignment by shifting individual maps axially, then radially, to match the mean map reduced overall variance. These transformations had very little effect on the population mean.

Conclusions. Simple transformations of individual GCL+IPL thickness maps to a canonical form can considerably reduce the population variance in a sample of normal eyes, likely improving the ability to discriminate abnormal maps. The transformations considered here preserve the local geometry of the thickness maps. When used on a patient's map, they can produce a deviation map that provides a meaningful measurement of the size of local thickness deviations and allows estimation of the number of ganglion cells lost in a glaucomatous defect. (*Invest Ophthalmol Vis Sci.* 2012; 53:3653–3661) DOI:10.1167/iovs.12-9719

Clinical methods for glaucoma diagnosis attempt to detect degenerative change, either in terms of functional damage (loss of visual sensitivity) or structural damage (tissue loss). To detect damage, measurements from a patient's eye are compared with values in a normative database to look for statistically significant deviation. Clearly, the lower the variance of the normal values, the more sensitive to change a measurement becomes.

Recent advances in optical coherence tomography (OCT) for glaucoma diagnosis have mostly focused on measurements of structure.[1] In particular, the cross-sectional and three-dimensional (3D) views provided by spectral domain OCT (SD-OCT) present new and more accurate ways to assess structural change. Structural measurements that are clinically relevant to glaucoma diagnosis include thickness of the peripapillary retinal nerve fiber layer (RNFL),[2,3] characteristics of the optic nerve head (ONH), such as cup to disc ratio and neural rim area,[2,4] and thickness of the inner layers of the macula.[2,5–8]

The ONH and peripapillary RNFL have anatomical variations among normal eyes that can add variance to a normative database. The ONH varies in size and shape, can tilt relative to the back of the eye, and has large retinal blood vessels through its center that obscure structural detail.[3] The peripapillary RNFL, although composed of approximately radial nerve fiber bundles that converge on the ONH, varies in the precise orientation of these bundles. In addition, the bundles can gather into inferior or superior bifurcations to produce local variations that are particularly evident on peripapillary thickness profiles.[9] Neither the ONH nor RNFL can be described by a simple spatial template.

In contrast to the ONH and RNFL, the inner layers of the macula, the ganglion cell layer (GCL), and the inner plexiform layer (IPL), have a less varied configuration. It is difficult to obtain meaningful measurement of these two layers individually, because the difference in their scattering properties is relatively small and, typically, not well resolved by commercially available OCT instruments, so this study focused on the sum of the two layers (GCL+IPL). In normal eyes, the GCL+IPL forms a thickened, approximately elliptical annulus that reflects the distribution of ganglion cells.[7,10,11] Although the macular GCL+IPL and the so-called ganglion cell complex (GCC; GCL+IPL+RNFL) are used in glaucoma diagnosis,[5,6] there have been no attempts to exploit the apparent symmetry of these structures to reduce variance in a normative database.

On the hypothesis that it is possible to define a canonical form for the normal GCL+IPL; that is, a standard template that accounts for a large share of the spatial variation in GCL+IPL thickness in the population, the similarities and differences in the shape of the normal macular GCL+IPL among individuals were examined. Two principal differences were found: foveal size and overall thickness. Simple spatial transformations of individual maps that can adjust for these differences and reduce the variance of a population of normal eyes were also found.

From the [1]Bascom Palmer Eye Institute, University of Miami Miller School of Medicine, Miami, Florida; and the [2]Department of Ophthalmology, University of North Carolina School of Medicine, Chapel Hill, North Carolina.

Supported by grants from the National Institutes of Health (P30EY014801), the Department of Defense (#W81XWH-09-1-0675), and an unrestricted grant from the Research to Prevent Blindness.

Submitted for publication February 17, 2012; revised April 19, 2012; accepted April 21, 2012.

Disclosure: **R.W. Knighton**, Carl Zeiss Meditec, Inc. (C), P; **G. Gregori**, Carl Zeiss Meditec, Inc. (F), P; **D.L. Budenz**, Carl Zeiss Meditec, Inc. (F)

Corresponding author: Robert W. Knighton, 2011 Featherstone Drive, Duluth, MN 55803; rknighton@med.miami.edu.

Methods

Subjects

Subjects who were participants in another study,[7] and who were healthy according to its criteria, were recruited to have extra SD-OCT scans of their maculas. Patients with glaucoma were also recruited. After explanation of the nature and possible consequences of the study, all subjects provided informed consent to participate. The study was approved by the institutional review board of the University of Miami and adhered to the tenets of the Declaration of Helsinki.

Normal data were initially available from both eyes of 47 subjects. To conserve time and labor, this study was limited to right eyes only. A preliminary estimate of foveal diameter (Fig. 1) was used to sort the eyes by foveal size, and an effort was made to select eyes that represented the entire range with approximately equal numbers of male and female subjects. Fourteen eyes were rejected outright; 3 were missing some element of data, and another 11 showed small eye movements that may have distorted the macular architecture. The final dataset comprised the right eyes of 23 subjects, 11 females and 12 males. The 10 eyes not included comprised three females and seven males. The ages of the 23 subjects ranged from 18 to 75 years, with a median age of 48 years.

Macular Imaging and GCL+IPL Thickness Maps

Macular SD-OCT imaging was performed with a Cirrus HD-OCT (Carl Zeiss Meditec, Dublin, CA). The 3D images contained 512 × 128 × 1024 voxels that sampled a 6 × 6 × 2-mm region (horizontal × vertical × depth) centered on the macula. The retinal layers were outlined by a combination of automatic and manual segmentations (Fig. 1). Automatic algorithms located the inner limiting membrane (ILM) and retinal pigment epithelium (RPE). The RNFL and IPL outer boundaries were manually segmented on selected b-scans using an interactive pen display (Cintiq 12WX, Wacom Technology Corp., Vancouver, WA). Where the RNFL and IPL vanished in the fovea, their boundaries were made to coincide with the ILM. The junction between inner and outer segments (IS/OS) was determined by automatic segmentation over a 1.8 × 1.8-mm central area. The location of the foveal center was defined as the point of maximum OS length, as determined on a smooth surface fit to the difference between IS/OS and RPE segmentations. All automatic segmentations were confirmed as reasonable by visual inspection.

Retinal blood vessels located in the RNFL and GCL challenge both automatic and manual segmentation algorithms and can confound measurements of GCL+IPL thickness. To address this problem, an OCT fundus image of the dataset was used to generate a binary mask of the blood vessel shadows that removed areas near and under vessels from the analysis. Briefly, a high-contrast fundus image of the vessel shadows was formed by axial summation across a slab of retina that straddled the RPE.[12] A rotating matched filter approach was used to detect vessel shadows,[13] a binary image was generated by interactively applying a threshold, then standard image processing operations[14] were applied to remove extraneous spots and fill holes in vessel shadows. Finally, the areas marked as vessel shadows were enlarged somewhat to include retina that may have contained vessel walls.

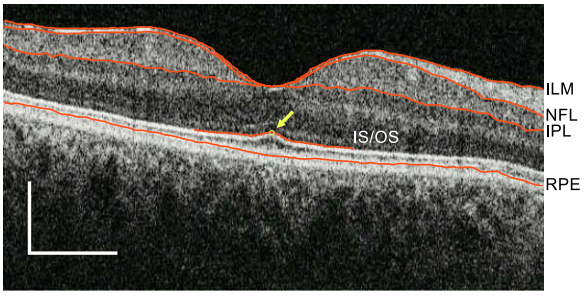

Figure 1. Layer segmentations (*red lines*) of a 6-mm long, horizontal b-scan through the fovea of a right eye. ILM, inner limiting membrane; NFL, outer margin of the retinal nerve fiber layer; IPL, outer margin of the inner plexiform layer; IS/OS, inner edge of the junction between photoreceptor inner and outer segments; RPE, retinal pigment epithelium. The *yellow circle* indicated by the *arrow* is the foveal center. Calibration bar equals 200 μm vertical, 1 mm horizontal.

Figure 2A shows an example of the measured GCL+IPL thickness data, where the thickness of the GCL+IPL was taken as the axial distance between manually segmented outer boundaries of the RNFL and IPL. Only every other b-scan was segmented except near the fovea, resulting in the horizontal striped appearance. The mask formed from blood vessel shadows produced a black branching pattern where data were excluded.

The GCL+IPL thickness data were converted to polar coordinates by nearest neighbor interpolation and represented by a smooth analytic surface generated with two-dimensional penalized splines (2D P-splines) (Fig. 2B).[15–17] The polar coordinate system was centered on the previously determined foveal center (Fig. 1), radial coordinates extended from 0.1 to 3.0 mm and angular coordinates extended from −180° to +180°, with 0° oriented nasally. This choice of coordinates recognized the apparent symmetry of the macula and respected the underlying anatomy of the GCL, in that the discontinuity at ±180° was approximately aligned with the temporal raphe[18] (in a left eye the angular coordinates would be mirror symmetric to those in Fig. 2B). The 2D P-spline fit approximates the data by the coefficients of a set of localized 2D basis functions, with the value of each coefficient being supported by a subset of the original data.[15–17] The basis functions are tensor products of B-splines, smooth curves formed from piecewise continous segments of polynomials, with penalties applied in each direction to the differences between adjacent coefficients. This work used an array of 16 quartic B-splines with a penalty of 0.2 in the radial direction, and 39 cubic B-splines with a penalty of 3.0 in the angular direction (624 coefficients). The fit produced a surface defined over the entire coordinate grid, including the areas with no data in Figure 2A. For the 23 eyes studied, the SE of the fit was 5.25 ± 0.38 μm. Thus, the average scatter of the data around the smooth surface had a magnitude similar to the axial resolution of the SD-OCT instrument. After the original thickness data had been fit, only the smooth surfaces were used in further analyses.

An additional set of SD-OCT images of the macula comprising 200 × 200 a-scans were available for 46 right eyes and 47 left eyes. These images were acquired at the same time as the 512 × 128 images analyzed here. The GCL+IPL thickness and foveal center for each image were obtained with proprietary algorithms included in the Cirrus HD-OCT commercial software and were converted to smooth surfaces in polar coordinates for analysis. For right eyes, these surfaces were used to make a preliminary estimate of foveal size to assist the selection of eyes for manual segmentation. For left eyes, these surfaces were used in a normative dataset to illustrate an application to glaucoma diagnosis of the methods developed here (see Discussion). To determine if the subset of 23 right eyes selected for manual segmentation was a reasonably representative sample of the available data, the 200 × 200 images also were used to compare the mean map of the subset (analogous to Fig. 3) to the mean map of all 46 right eyes. On average, the two mean maps differed by 0.11 ± 0.58 μm, with no points differing by more than ±2.5 μm.

All data fitting and analyses were carried out using custom programs written in MATLAB (The MathWorks, Natick, MA). Descriptive statistics are reported as mean ± one SD.

Results

Mean and Variance of GCL+IPL Thickness

The overall similarities and differences of the macular GCL+IPL thickness among eyes can be appreciated by examining mean

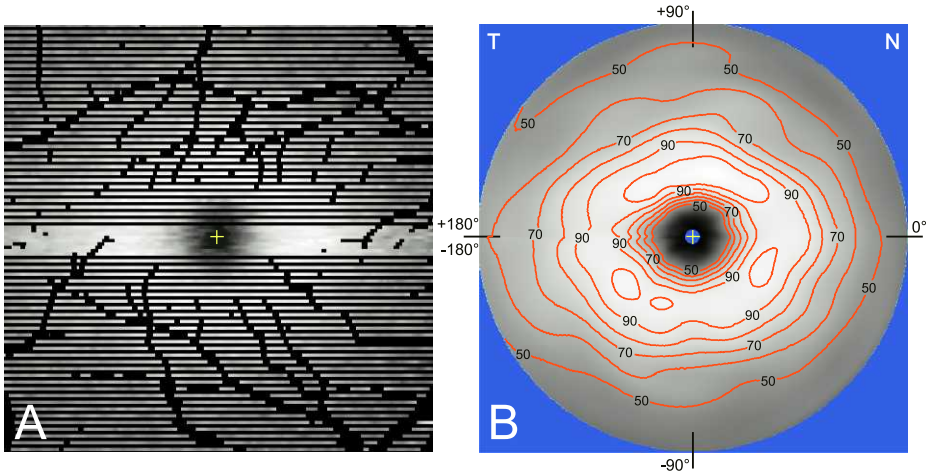

Figure 2. Representation by a smooth surface of GCL+IPL thickness data from a right eye. The *yellow cross* in each image marks the point of maximum OS length, which was assumed to be the foveal center. (**A**) Original thickness data from a 512 × 128 macular scan covering a 6 × 6-mm retinal area. *Black areas* correspond to missing data, either because some b-scans were not segmented, or due to the presence of blood vessels. (**B**) The data in (**A**) fit by a smooth surface in polar coordinates centered on the fovea. Horizontal and vertical meridians are labeled at the image edge. The nasal and temporal edges are marked N and T, respectively. *Blue areas* indicate data that are not represented in polar coordinates. The contour interval is 10 μm, with every other contour labeled.

and variance maps for the 23 right eyes studied (Fig. 3). These were easily produced from the fitted surfaces, because in polar coordinates the maps for individual eyes were already aligned on the fovea.

The mean thickness map had an approximately elliptical symmetry centered on the fovea, as shown by the contour map in Figure 3A. With increasing radial distance from the fovea, the thickness increased to a peak and then slowly decreased, forming a broad ridge surrounding the fovea. The peak of this macular ridge was temporally thinner compared with elsewhere, consistent with GCL asymmetry shown by histology[10,19] and OCT,[11] but, otherwise, the mean thickness map was remarkable for its simplicity. The two contour lines highlighted in Figure 3A serve to relate features of the mean map to corresponding locations on the SD map. The outer 90-μm contour falls on the outer slope of the macular ridge, and the inner 50-μm contour falls on the rising foveal edge. The 50-μm contour on the foveal edge also provided a means to measure foveal size; the foveal size was defined as the average radius of the inner 50-μm contour. Defined this way, the mean foveal size of the 23 study eyes was 0.44 ± 0.08 mm. These

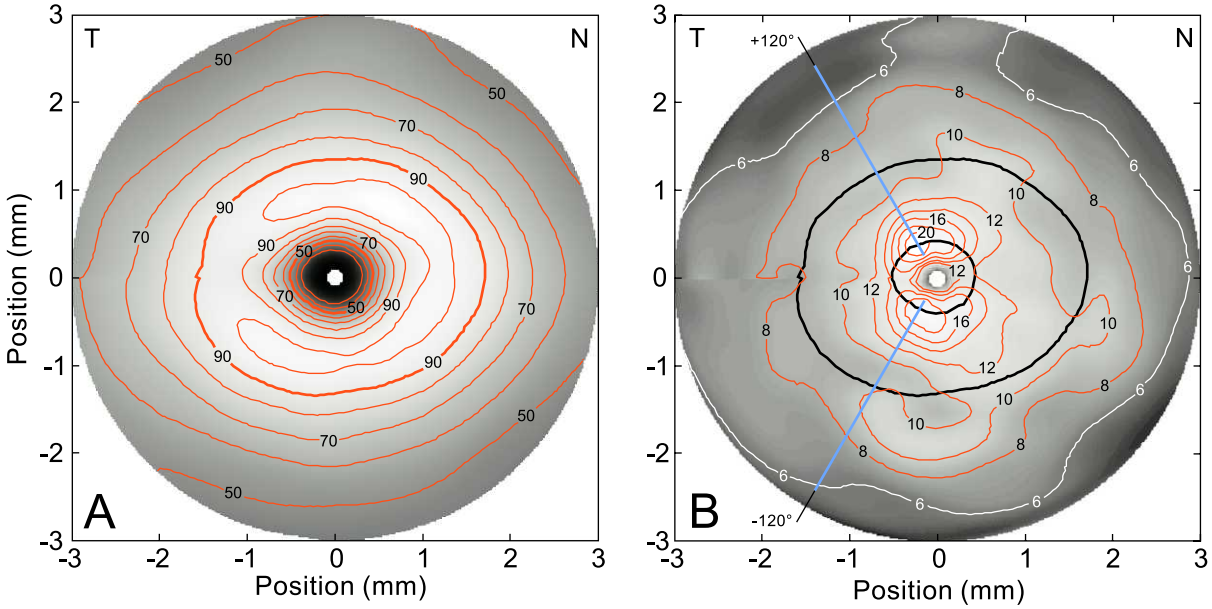

Figure 3. The mean and variance of the GCL+IPL thickness of 23 normal right eyes created from smooth fits in polar coordinates. (**A**) Mean map. The contour interval is 10 μm, with every other contour labeled. The inner 50-μm and outer 90-μm contours are highlighted with wider lines. (**B**) Standard deviation map. The values displayed are the square root of the variance (SD). Contour interval is 2 μm. The 6-μm contour line is drawn in *white* for better contrast. The *black lines* show the highlighted 50- and 90-μm contours in (**A**). The two *blue meridians* at ±120° pass through regions of high variance and mark the locations of profiles shown in Figures 5 and 6.

values are approximately the same as found for normal foveal profiles by Wang et al.[20]

The population variance for the 23 eyes is displayed in the map of Figure 3B. The SD (square root of the variance) increased from about 6 μm in the periphery to about 10 μm near the macular ridge, and then became considerably higher in the region between the macular ridge and the fovea. This area of higher SD occurred in a region of thick GCL+IPL where it could interfere with the detection of glaucomatous damage. Two regions with the highest variance lay near the meridians at ±120° (blue lines in Fig. 3B).

The sources of the overall population variance and the higher variance near the foveal edge are evident from the seven individual profiles in Figure 4A, which were selected to represent quantiles in foveal size; for example, the leftmost profile at 50 μm is from the smallest fovea, the rightmost is from the largest, and the other five profiles span the central 67% of the population. Not only did eyes vary in foveal size, but Figure 4A also shows that they varied in overall GCL+IPL thickness, presumably due to variation in the total number of ganglion cells.[10,19] This suggests that overall thickness variation generates most of the variance seen outside the macular ridge, but that the higher variance inside the macular ridge has an additional significant component due the variation in foveal size.

Figure 4B shows how a small change in foveal size can result in a large change in thickness at the foveal edge. The blue line is the +120° profile of the mean. To mimic differences in foveal size, this profile was shifted horizontally (radially) toward and away from the fovea by 1 SD of the foveal size (0.08 mm) to produce the red lines that intersect the two ends of the black horizontal error bar. Although this shift produced only a small thickness change at, and peripheral to, the profile peak, the double-headed arrow shows that it produced a very large thickness change at the foveal edge.

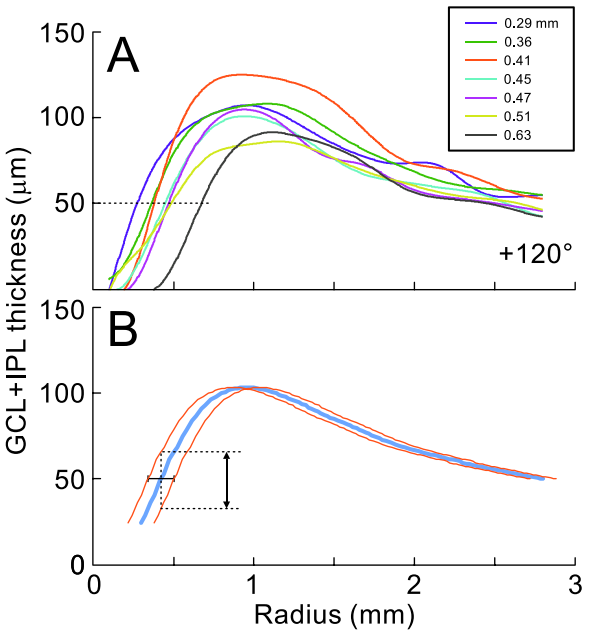

Figure 4. Source of variance in GCL+IPL thickness maps. (**A**) Thickness profiles along the +120° meridian from seven eyes, selected to span the range of foveal sizes. The *dotted line* shows where the 50-μm level crosses the foveal edge. The *inset* gives the foveal size for each eye. (**B**) Conceptual diagram of the effect of foveal size on population variance. The *blue line* is the +120° profile of the mean map and the *black horizontal error bar* shows ±1 SD of the foveal size. The *red lines* are the same profile shifted toward and away from the fovea. The *double-headed arrow* shows the difference in thickness between the two *red* profiles.

Foveal Size Correction

The effect on variance of small shifts in radial profiles (Fig. 4B) suggested that perifoveal variance could be reduced by radially shifting individual maps to correct for differences in foveal size. Radial shifting was easily implemented in polar coordinates. The foveal size (mean radius of the foveal edge) was determined for each eye and for the population mean. Then, for each eye the surface in polar coordinates was shifted in the radial direction by an amount that made its foveal size equal to the foveal size of the population mean. Thus, eyes with larger foveas had all points shifted radially toward the center, and eyes with smaller foveas had all points shifted radially away from the center. The set of shifted surfaces was then used to form new population mean and variance maps. Foveal size correction produced little change in the mean map (mean difference = −0.08 ± 0.36 μm). It appeared identical to Figure 3A and is not shown. The variance is shown in Figure 5A as a SD map. A radial shift leaves one edge of a polar map without data, so the area of overlap between maps is smaller than the original map area. The limits of data overlap determined by the maximum inward and outward shift values are shown as dotted circles in Figure 5A.

Comparing the fovea-corrected SD map in Figure 5A with the original SD map in Figure 3B shows that foveal size correction had little effect on the variance outside the macular ridge. Inside the macular ridge, however, the correction for foveal size reduced the variance substantially, to values similar to peripheral retina. This reduction in variance extended over the entire foveal slope. The GCL+IPL thickness profiles in Figures 5B and 5C show another view of this variance reduction. The blue lines show the mean ±1 SD before, and the red lines show the result after foveal size correction. Three features of these profiles are evident: first, the corrected mean hardly differed from the original mean; second, the peripheral variance changed little; and third, the perifoveal variance after correction was considerably smaller than before.

Thickness Alignment

Two factors contributing to the variance seen in Figure 5 were the interindividual differences in overall GCL+IPL thickness and the intraindividual deviations from the shape of the common mean. To reduce the contribution of the overall difference, each individual map was aligned to the map of the population mean (Fig. 3A) by minimizing the volume of the difference between them, while imposing a constraint on the foveal size. The volume difference was calculated over an annulus with radii of 0.3 and 2.6 mm (dashed yellow circles in Fig. 6A), and the alignment was done using an iterative procedure that, at each step, shifted the individual map first in thickness, then radially. Because a shift in thickness is along the direction of the OCT scan beam, it will be called axial shifting. After alignment, each individual map had the same foveal size and overall thickness as the mean map.

The mean of the thickness-aligned maps was very nearly the same as the mean map of the original data (Fig. 3A; mean difference = 0.01 ± 0.36 μm) and is not shown separately. Figure 6A shows the SD of the thickness-aligned maps and Figures 6B and 6C show two thickness profiles. As seen by comparing Figures 3B, 5, and 6, the variance of the thickness-aligned maps was reduced almost everywhere. The axial shifting reduced variance at, and peripheral to, the macular

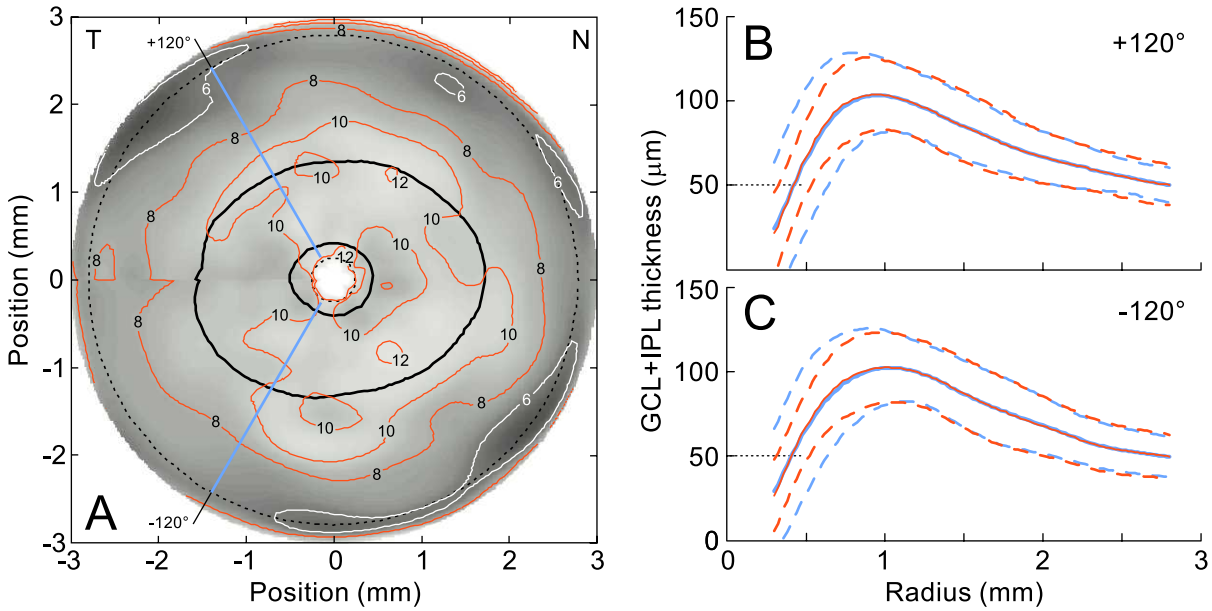

Figure 5. (**A**) The SD map for the GCL+IPL thickness of 23 right eyes after undergoing foveal size correction. This image uses the same gray scale as Figure 3B. The *black lines* show the highlighted 50- and 90-µm contours from Figure 3A. The *thin dotted circles* show the limits of overlap of the shifted data. (**B**, **C**) Thickness profiles along two meridians in (**A**) (*red*) superimposed on profiles from the same meridians in Figure 3 (*blue*). *Dashed lines* show ±1 SD of the two profiles.

peak, while radial shifting retained the variance reduction around the foveal edge produced by foveal size correction.

Discussion

Macular Analysis Methods

Three features of the analyses reported here deserve comment. First, the use of 2D P-splines offered a convenient mathematical formalism with which to manipulate the data. This approach to fitting a smooth surface captured most of the meaningful variation in the data with a limited number of coefficients, while also providing a means to control the amount of smoothing.[15–17] Furthermore, individual coefficients represented local areas of a map, making the method well suited for a disease with localized defects, such as glaucoma. Eventually, the number of coefficients and degree of smoothing chosen for a clinical application can be guided by

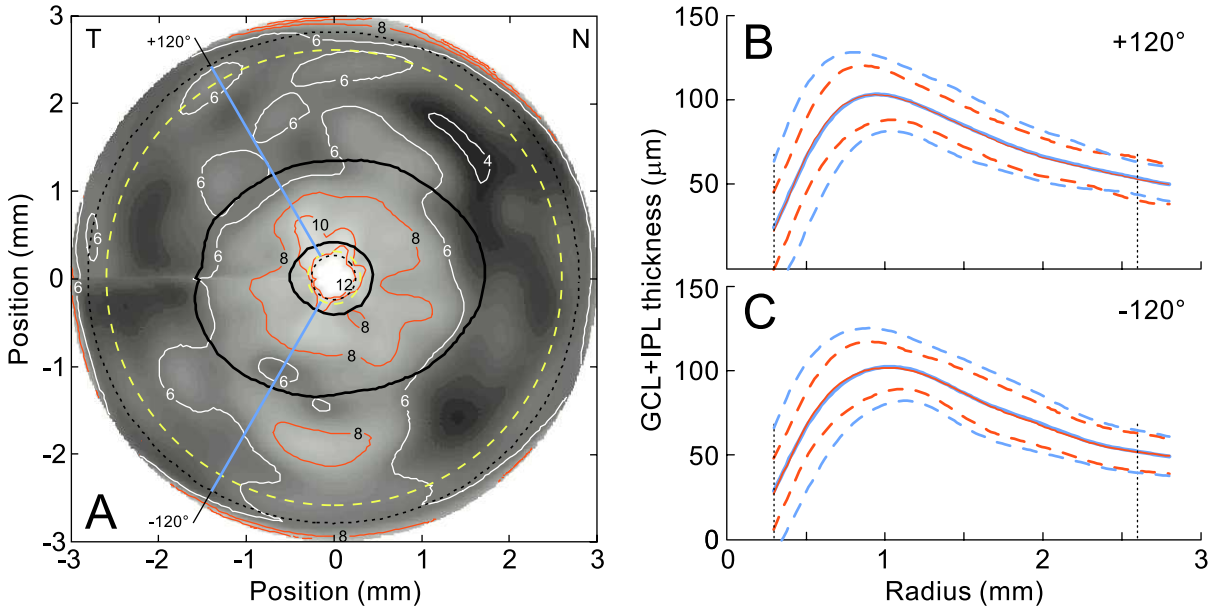

Figure 6. (**A**) The SD of the maps formed by thickness alignment. This image uses the same gray scale as Figures 3B and 5A. The *dashed yellow lines* show the inner and outer boundaries of the annulus used for aligning individual maps to the population mean. The *black lines* and *thin dotted circles* are as in Figure 5A. (**B**, **C**) Thickness profiles along two meridians in (**A**) (*red*) superimposed on profiles from the same meridians in Figure 3 (*blue*). *Dashed lines* show ±1 SD of the two profiles. *Dotted vertical lines* show the limits of the annulus used in thickness alignment.

the size of structural damage usually found in glaucoma. It is worth noting, however, that the variance reduction methods presented here do not depend on the use of P-splines. Radial and axial shifting can be applied to other smoothed or interpolated representations of the data to achieve the desired transformations.

The second analysis feature was the removal of areas containing blood vessels with the goal of improving the accuracy of the GCL+IPL thickness data. Retinal blood vessels, especially larger vessels, are likely to add uncertainty to the actual thickness value in their vicinity. Vessels may mechanically distort the GCL and IPL, and affect the contrast between different layers. For instance, in the case of the RNFL they often confound expert manual identification of the anatomical boundary as well as segmentation algorithms,[6,21] and add nonneural tissue to the thickness.[22,23] Applying a vessel mask before smoothing should remove this uncertainty, and provide a fitted surface that depends only on the data between vessels. The vessel mask may be especially useful to detect tissue loss; a thickness change due to glaucoma will not be diluted by the presence of the more stable blood vessels.

The third analysis feature was the use of a polar coordinate system centered on the fovea and oriented to respect the temporal raphe. The temporal raphe, the anatomical line of separation between ganglion cells serving superior and inferior retina,[18] is the expected location for a structural step that corresponds to the commonly seen nasal step in glaucomatous visual fields. Placing the $\pm 180^{\circ}$ angular limits along the temporal meridian and, thus, at the approximate location of the temporal raphe ensured that data points above and below the temporal meridian did not interact mathematically when a smooth surface was generated. Biological variation in the temporal raphe and uncontrolled ocular rotation, however, make exact alignment of the coordinate system with anatomy difficult. Data from the SD-OCT scan pattern that were not represented in the polar coordinate system (blue center and corners in Fig. 2B) have a thinner GCL,[10] and are arguably less important for GCL+IPL assessment in glaucoma diagnosis. In addition to conforming to macular anatomy, the use of polar coordinates also facilitated the radial shifting method of foveal size correction.

Canonical Form for GCL+IPL Thickness

This study quantified the similarities and differences in macular GCL+IPL thickness in a group of healthy individuals in order to understand various contributions to their population variance. The GCL+IPL thickness maps of the 23 maculas in this study all had a similar topography, exemplified by the mean map in Figure 3A. The two main differences between individual maps were foveal size and overall thickness (Fig. 4A), which caused much of the variance displayed in Figure 3B. Simple transformations can produce canonical versions of each individual map having the same foveal size, or the same overall thickness, or both the same foveal size and overall thickness, as the mean map. An important feature of these transformations is that they preserve the local geometry of the individual thickness maps and their population mean, while greatly reducing the population variance.

The two transformations used here, radial and axial shifting, do not remove all known differences in the shapes of individual, normal maculas. In particular, the macular ridge and the 50-μm contour on the foveal edge can be well fit by ellipses that vary in elongation and tilt between individuals (manuscript in preparation). Whether a suitable transformation could improve the alignment of this elliptical component and further reduce variance in a normative dataset requires more study. Ultimately, however, normal individual deviations from a common shape and uncontrolled variations in data acquisition, such as ocular torsion and head tilt, will impose a limit on the utility of transformation to a canonical form for the purpose of reducing population variance.

Foveal Size Correction by Radial Shift Transformation

The two transformations that produced the reduced variance seen in Figures 5 and 6 should prove useful for improving glaucoma diagnosis. The first transformation, a radial shift in polar coordinates, provided a robust method for aligning the rising edge of an individual, normal fovea to the foveal edge of the population mean. For the purpose of this analysis, the foveal edge was located by the 50-μm contour line, which in normal eyes lies within the region of maximum slope. Foveal size then was defined to be the mean radius of the 50-μm contour. Foveal size varied over a 2 to 1 range in the 23 eyes studied, with an SD of 18% of the mean (Fig. 4A). Figure 4B shows how this amount of variation in the steeply rising foveal edge could produce a large variation in perifoveal GCL+IPL thickness. Use of a radial shift to correct for foveal size was especially effective because the locations of the foveal edge and the macular ridge are well correlated with unity slope (manuscript in preparation). Thus, the concept of shifted profiles, as depicted in Figure 4B, is a reasonable approximation to the behavior of a population of actual maculas, allowing the radial shift transformation to greatly reduce the perifoveal variance without significantly affecting the peripheral variance (Fig. 5).

The mean radius of the 50-μm contour line of the GCL+IPL thickness maps is a simple estimate of foveal size based on the average geometry of normal foveas (manuscript in preparation) that proved to be effective (Fig. 5). In eyes with advanced disease, however, this estimate of foveal size may be biased. Although it may be possible to adopt a more intrinsic definition of foveal size, whether such a choice would significantly affect the sensitivity and specificity of the definition used here is beyond the scope of this article. It also must be remembered that the concept of foveal size correction provides a tool to improve the discrimination of damaged from normal eyes. Disease so advanced that a simple definition of foveal size becomes unusable is expected to be detected without foveal size correction.

Foveal morphology varies with race and sex[24,25] and various macular thickness parameters vary with foveal size.[11,24,25] As a consequence OCT normative databases are often stratified by race and sex.[7] Variance reduction by foveal size correction may reduce the need for such stratification. Correction for foveal size may also provide a way to compensate for magnification differences due to differences in axial length. It should be possible to test these ideas on existing normative databases.

Thickness Alignment by Axial Shift Transformation

The second transformation, axial shifting, is a novel method for aligning an individual map to a reference map so they have the same average thickness. In this study axial and radial shifting were combined in a thickness alignment procedure that transformed each individual map to a canonical form with the same foveal size and overall thickness as the mean map. This thickness-aligned map can be used for glaucoma diagnosis by subtracting the normal mean map to form a thickness deviation (TD) map. With overall thickness differences removed, a TD map emphasizes deviation from normal shape. Performing a statistical comparison using a reduced variance normal map, such as Figure 6A, could provide a more sensitive

Table 1. Data Values at the Peaks of the Horizontal Meridian

			Nasal	Temporal	No. of Eyes	Source
1	GC density (GCs/mm^2)		31.6×10^3	26.9×10^3	5	Fig. 6; Ref. 10
2	GCL thickness (μm)		71	57	18	Fig. 7; Ref. 19
3	GCL+IPL thickness (μm)	Histology	107	93	18	Fig. 7; Ref. 19
4		OCT	101.5	93.6	23	Fig. 3A

approach to the detection of localized damage. The TD map is somewhat analogous to the pattern deviation (PD) map proposed by Tan et al.,[6] except that the PD map uses multiplicative scaling to normalize both the individual map and the normal reference map before subtraction (the PD map also does not correct for foveal size). Normalization by scaling reduces the relative amplitude of a deviation in a thicker than average map and increases it in a thinner than average map, leading to false negative comparisons in the first case and false positive ones in the second. In contrast, a TD map preserves the amplitude of deviations regardless of the overall thickness of the map being compared.

The fact that an axial shift preserves local geometry has an important property: GCL+IPL volume is the product of thickness and area, so that TD averaged over a given region is a direct measure of volume deviation in that region (neglecting the effect of blood vessel removal) (Fig. 2A). On the assumptions that in glaucoma (1) ganglion cells do not change volume; (2) other cells do not invade the GCL; and (3) IPL thickness does not change, the volume deviation is proportional to the number of ganglion cells by which a given individual map differs from the mean map. The three assumptions listed are probably not strictly correct, but may be correct enough for the concept to have clinical utility. Thus, TD can be considered directly proportional to the number of ganglion cells lost in a region, and may provide a natural and intuitive way to discuss structural changes in glaucoma.[26] Moreover, the idea of expressing glaucomatous loss in terms of ganglion cell number can be extended to any thickness difference, whether one is talking about overall loss from normal deviations, from normal shape, or loss over time.

An estimate of the proportionality constant that links OCT thickness to ganglion cell number was attempted by using data for the peaks of macular thickness profiles along the horizontal meridian. Histologic data for the GCL and IPL at the macular peaks are available from Curcio and Allen[10] and Curcio et al.[19] The mean map in Figure 3A provides values for the OCT thickness of GCL+IPL. In each case, these peaks represent averages from several eyes. The relevant data are assembled in Table 1.

Using the data in Table 1, Row 1 was divided by Row 2, which yielded histologic GC volume densities (GC areal density per GCL thickness) of 445 and 472 GCs/mm^2 per μm for the nasal and temporal peaks, respectively, for an average of 458 GCs/mm^2 per μm. Similarly, GCL+IPL thicknesses at the peaks of the histologic and OCT profiles (Rows 3 and 4) average to give 0.98 for the ratio OCT: histologic thickness, which may represent the average change in the tissue due to postmortem swelling followed by shrinkage due to histologic preparation.[19] Combining the preceding values yields a working estimate for the GC loss coefficient of 449 GCs/mm^2 for each micrometer of OCT thickness loss. More accurate values for the entries in Table 1 would, of course, improve this estimate.

An Example

To demonstrate how variance reduction in a normative database might aid the detection of glaucomatous damage, a 200 × 200 SD-OCT image was selected from the left eye of a 44-year-old female patient with mild glaucomatous damage, as determined by examination of the visual field and optic nerve head. This eye had a visual field mean deviation of −1.15 dB. It also had a thicker than average overall GCL+IPL thickness, and a smaller than average foveal diameter, characteristics that increased the likelihood that it would appear normal using current structural measures.

The normative dataset consisted of 200 × 200 SD-OCT images of the 47 left eyes of our original subject population.

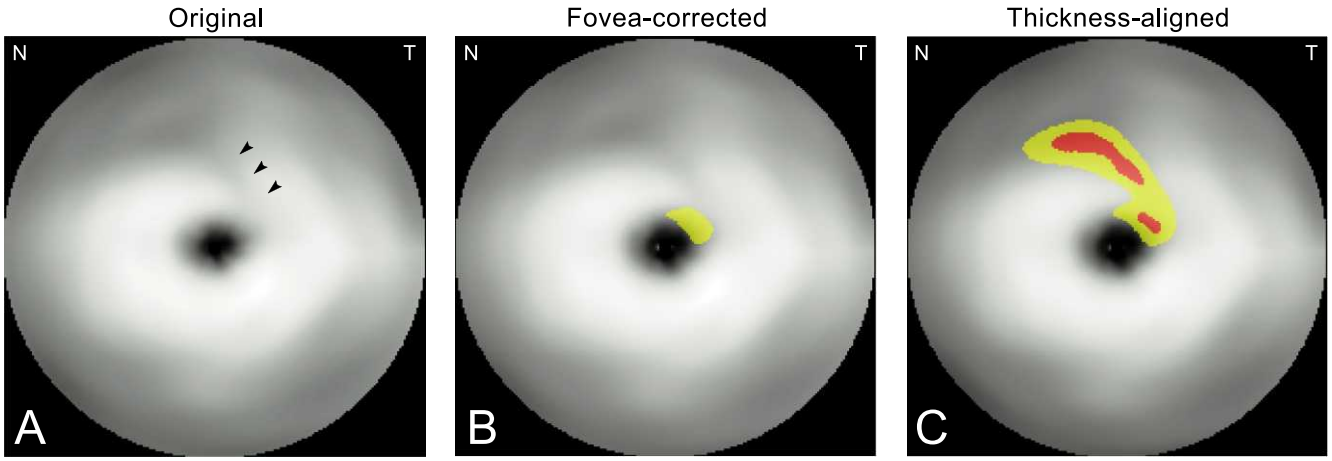

Figure 7. Three different forms of the GCL+IPL thickness map of the left eye of a glaucoma patient compared with their respective normative datasets. Areas that fall significantly below the mean are highlighted in *yellow* (−2 SD) and *red* (−3 SD). (**A**) Original patient map compared with Original Normal map. The *arrowheads* indicate an area of possible damage that does not reach statistical significance. (**B**) Fovea-corrected patient map compared with Fovea-corrected Normal map. A notch on the foveal slope falls more than 2 SD below normal. (**C**) Thickness-aligned patient map compared with Thickness-aligned Normal map. An arcuate area deviates significantly from the normal shape.

This dataset was used to generate three GCL+IPL mean thickness maps and their associated variance maps: the Original Normal map (with variance analogous to Fig. 3B), the Fovea-corrected Normal map (with variance analogous to Fig. 5A) formed by radially shifting the 47 individual maps to have the same foveal size as the Original Normal map, and the Thickness-aligned Normal map (with variance analogous to Fig. 6A) formed by thickness alignment of the individual maps to the Original Normal map. A three-step procedure is proposed to compare the patient's image to the normative dataset.

The patient map with appropriate transformations was compared with each of the normal maps in turn (Fig. 7). Yellow areas in Figure 7 indicate deviations greater than 2 SD below normal, and red areas indicate deviations greater than 3 SD below normal. In the first step, when compared with the Original Normal map (Fig. 7A) the original patient map showed no significant deviation, although a superior area did appear thinner than its surroundings (arrowheads). Here, it should be noted that if in the first comparison a patient map differs greatly from normal (e.g., 3 SD below normal over a large enough area), no further comparison is needed; the patient map has been identified as abnormal with no need for further steps to reduce variance. Indeed, one can imagine cases where large but symmetric deviations from normal, such as a 360° perifoveal loss or uniform overall thickness loss, might be detected in the first comparison but obscured by subsequent transformation.

In the second step, the foveal size of the patient map was measured and a radial shift was applied to equate it with the Fovea-corrected Normal map, yielding the map in Figure 7B. In this case, the shift was away from the foveal center, and the foveal depression in Figure 7B appears larger than in Figure 7A. In this step, the equal foveal sizes and reduced perifoveal variance of the Fovea-corrected Normal map revealed a small abnormal notch on the foveal slope of the patient map (yellow patch adjacent to the foveal depression).

Because the Fovea-corrected Normal map retains the population variance in overall thickness, in most cases, it shares the capability to detect diffuse loss of GCL+IPL thickness with the Original Normal map; that is, an overall thickness that falls significantly below normal. No diffuse loss was apparent in this patient's macula.

The third, and final, diagnostic step was to look for local deviations of the patient map from the normal shape of the GCL+IPL. To do this, the patient map was transformed by axial and radial shifting and compared to the Thickness-aligned Normal map. This revealed an arcuate region (highlighted yellow and red in Fig. 7C) that deviated significantly from the normal macular shape, strongly suggesting the presence of glaucomatous damage. The highlighted region had an average thickness loss of 18.2 μm and an area of 1.97 mm^2. Applying the GC loss coefficient of 449 GCs/mm^2 per μm yields an estimated loss of about 16,100 GCs for the arcuate defect of Figure 7C.

This particular example was selected to demonstrate the increase in sensitivity for glaucoma detection that might result from this approach to reducing the variance of a normative database of GCL+IPL thickness maps. A thorough evaluation of the performance of the proposed protocol will require a careful study using large normative databases, and representative populations of patients with varying degrees of glaucoma.

Conclusion

Simple transformations to a canonical form of individual, normal GCL+IPL thickness maps can yield a normative database with reduced variance that should improve glaucoma diagnosis. Applying the same transformations to a patient's map, and comparing it to the appropriate normative database can produce a TD map that preserves the size of local TDs, and allows estimation of the number of ganglion cells lost in a glaucomatous defect.

Acknowledgments

The authors thank Xiangrun Huang for providing the method used to form the blood vessel masks.

References

1. Gabriele ML, Wollstein G, Ishikawa H, et al. Optical coherence tomography: history, current status, and laboratory work. *Invest Ophthalmol Vis Sci*. 2011;52:2425–2436.
2. Rao HL, Zangwill LM, Weinreb RN, Sample PA, Alencar LM, Medeiros FA. Comparison of different spectral domain optical coherence tomography scanning areas for glaucoma diagnosis. *Ophthalmology*. 2010;117:1692–1699.
3. Leite MT, Rao HL, Zangwill LM, Weinreb RN, Medeiros FA. Comparison of the diagnostic accuracies of the Spectralis, Cirrus, and RTVue optical coherence tomography devices in glaucoma. *Ophthalmology*. 2011;118:1334–1339.
4. Sharma A, Oakley JD, Schiffman JC, Budenz DL, Anderson DR. Comparison of automated analysis of Cirrus HD OCT spectral-domain optical coherence tomography with stereo photographs of the optic disc. *Ophthalmology*. 2011;118:1348–1357.
5. Kotera Y, Hangai M, Hirose F, Mori S, Yoshimura N. Three-dimensional imaging of macular inner structures in glaucoma by using spectral-domain optical coherence tomography. *Invest Ophthalmol Vis Sci*. 2011;52:1412–1421.
6. Tan O, Chopra V, Lu AT, et al. Detection of macular ganglion cell loss in glaucoma by Fourier-domain optical coherence tomography. *Ophthalmology*. 2009;116:2305–2314.
7. Mwanza JC, Durbin MK, Budenz D, et al. Profile and predictors of normal ganglion cell-inner plexiform layer thickness measured with frequency-domain optical coherence tomography. *Invest Ophthalmol Vis Sci*. 2011;52:7872–7879.
8. Asrani S, Rosdahl JA, Allingham RR. Novel software strategy for glaucoma diagnosis: asymmetry analysis of retinal thickness. *Arch Ophthalmol*. 2011;129:1205–1211.
9. Ghadiali Q, Hood DC, Lee C, et al. An analysis of normal variations in retinal nerve fiber layer thickness profiles measured with optical coherence tomography. *J Glaucoma*. 2008;17:333–340.
10. Curcio CA, Allen KA. Topography of ganglion cells in the human retina. *J Comp Neurol*. 1990;300:5–25.
11. Ooto S, Hangai M, Tomidokoro A, et al. Effects of age, gender, and axial length on the three-dimensional profile of normal macular layer structures. *Invest Ophthalmol Vis Sci*. 2011;52:8769–8779.
12. Jiao S, Knighton R, Huang X, Gregori G, Puliafito CA. Simultaneous acquisition of sectional and fundus ophthalmic images with spectral-domain optical coherence tomography. *Opt Express*. 2005;13:444–452.
13. Chaudhuri S, Chatterjee S, Katz N, Nelson M, Goldbaum M. Detection of blood vessels in retinal images using two-dimensional matched filters. *IEEE Trans Med Imaging*. 1989;8:263–269.
14. Gonzalez RC, Woods RE, Eddins SL. *Digital Image Processing Using MATLAB®*. 2nd ed. Gatesmark, LLC; 2009.
15. Eilers PHC, Marx BD. Flexible smoothing with B-splines and penalties. *Stat Sci*. 1996;11:89–121.
16. Eilers PHC, Currie ID, Durban M. Fast and compact smoothing on large multidimensional grids. *Comput Statist Data Anal*. 2006;50:61–76.

17. Currie ID, Durban M, Eilers PHC. Generalized linear array models with applications to multidimensional smoothing. *J R Statist Soc B*. 2006;68(Part 2):259–280.
18. Vrabec F. Temporal raphe of human retina. *Am J Ophthalmol*. 1966;62:926–938.
19. Curcio CA, Messinger JD, Sloan KR, Mitra A, McGwin G, Spaide RF. Human chorioretinal layer thicknesses measured in macula-wide, high-resolution histologic sections. *Invest Ophthalmol Vis Sci*. 2011;52:3943–3954.
20. Wang M, Hood DC, Cho JS, et al. Measurement of local retinal ganglion cell layer thickness in patients with glaucoma using frequency-domain optical coherence tomography. *Arch Ophthalmol*. 2009;127:875–881.
21. Mayer MA, Hornegger J, Mardin CY, Tornow RP. Retinal nerve fiber layer segmentation on FD-OCT scans of normal subjects and glaucoma patients. *Biomed Opt Express*. 2010;1:1358–1383.
22. Hood DC, Fortune B, Arthur SN, et al. Blood vessel contributions to retinal nerve fiber layer thickness profiles measured with optical coherence tomography. *J Glaucoma*. 2008;17:519–528.
23. Patel NB, Luo X, Wheat JL, Harwerth RS. Retinal nerve fiber layer assessment: area versus thickness measurements from elliptical scans centered on the optic nerve. *Invest Ophthalmol Vis Sci*. 2011;52:2477–2489.
24. Wagner-Schuman M, Dubis AM, Nordgren RN, et al. Race- and sex-related differences in retinal thickness and foveal pit morphology. *Invest Ophthalmol Vis Sci*. 2011;52:624–634.
25. Tick S, Rossant F, Ghorbel I, et al. Foveal shape and structure in a normal population. *Invest Ophthalmol Vis Sci*. 2011;52:5105–5110.
26. Harwerth RS, Wheat JL, Fredette MJ, Anderson DR. Linking structure and function in glaucoma. *Prog Retinal Eye Res*. 2010;29:249–271.